Optical and morphological characterization of Bi^{3+} doped zinc oxide and its solar photocatalytic application

BALASO JADHAV[a], ASHOKRAO PATIL[b], SATISH PARDESHI[c*]
[a]*Department of Chemistry, Sharadchandra Pawar Mahavidyalaya, Lonand (Shivaji University, Kolhapur), India*
[b]*Department of Chemistry, K.M.C. College, Khopoli (University of Mumbai), India*
[c]*Department of Chemistry, Savitribai Phule Pune University (formerly University of Pune), Ganeshkhind, Pune 411007, India*

Bi-doped ZnO(BZO) powders of different Bi contents have been synthesized by co- precipitation method and characterized by TG–DTA, XRD, FT Raman, XPS, SEM–EDX, UV–visible and photoluminescence (PL) studies. X-ray diffraction data suggests the hexagonal wurtzite structure for modified ZnO crystallites and the incorporation of Bi^{3+}expands the lattice constants of ZnO, while XPS spectra reveals the presence of Zinc and Bismuth in Zn^{2+} and Bi^{3+} oxidation states. The PL spectra suggest more number of oxygen vacancies in Bi-doped ZnO than bare ZnO. The photocatalytic performance of Bi-doped ZnO, compared to bare ZnO was examined by photo degradation (PCD) of Rhodamine 6G (Rh6G) in aqueous media under solar light. It has been found that Bi-doped ZnO showed better solar PCD efficiency than pristine ZnO.

(Received February 5, 2020; accepted February 15, 2021)

Keywords: Bi-doped ZnO, Co-precipitation, Sunlight, Photocatalysis, Rhodamine6G

1. Introduction

Zinc oxide is a unique semiconductor material having similar properties to TiO_2 with a characteristic direct and wide band gap (3.37 eV at room temperature) and large excitation binding energy of 60 MeV [1]. ZnO-based photo catalysts have been paid much attention because of its excellent properties, such as high chemical stabilization, non-toxicity, solar light activity and abundance in nature [2]. Heterogeneous photo catalysis with ZnO has been successfully applied to degrade organic pollutants [3]. Baruah *et al*. [4] have reported that heterogeneous photo catalytic systems via metal oxide semiconductors like TiO_2 and ZnO, are capable of operating effectively and efficiently for waste water treatment. Meng *et al*.[5] reported that ZnO is an excellent photo catalytic oxidation material. It has been usually used to deal with waste water, such as pharmacy waste water, printing and dyeing wastes, paper making waste water, and so on. The efficiency of photo catalytic degradation by ZnO should be improved further in order to meet the requirements of environmental protection.

The main factor influencing the photo catalytic activity of ZnO is reducing the rate of recombination processes of charge carriers. Therefore to improve the photo catalytic performance of bare ZnO different kinds of metal ion impurities were doped into ZnO which hinder the recombination of photo induced electrons and holes [6]. In particular the catalysts doped with cations of d^{10} electronic configuration for e.g. Bi^{3+}, In^{3+}, Al^{3+} and Ga^{3+} are most promising candidates. Among these, bismuth doped photo catalyst receive major attention. Bismuth is 83rd most abundant heavy element and is excellent alternative to noble metals since it is low cost, non-toxic and environmentally friendly material. Bi_2O_3 is a *p*-type semiconductor with band-gap energy of 2.85 eV, which can absorb a portion of visible light (≤440 nm) [7].It has been reported that, Bi^{3+} when incorporated into TiO lattice, enhances the spectral range of TiO_2 and prevents electron-hole recombination thereby facilitating photo catalytic performance [8,9]. Moreover doping of Bi^{3+} into ZnO is expected to shift the absorption edge of ZnO and the binding energy value of Zn $2p_{3/2}$ and influence the separation rate of photo induced charge carriers of ZnO because of the different structure of the electronic shell and size of Bi and Zn.

Rhodamine dyes namely Rhodamine B (RB, $C_{28}H_{31}N_2O_3Cl$), Rhodamine Blue (RBL, $C_{28}H_{32}N_2O_3$) and Rhodamine 6G (R6G, $C_{28}H_{31}ClN_2O_3$) belong to Xanthene class (Scheme 1) and are used as dye laser materials [10].

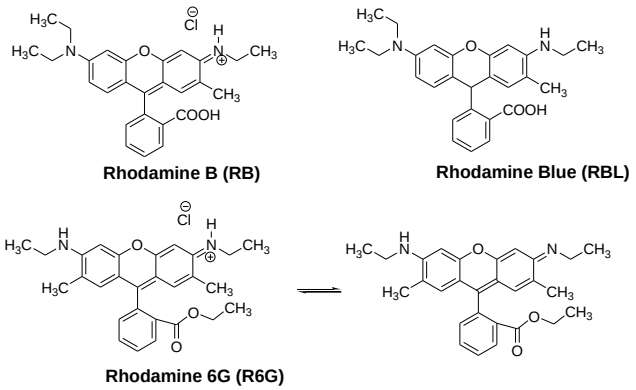

Scheme 1. Molecular Structures of Rhodamine (Xanthene) dyes

Among these dyes Rhodamine 6G is a chromophoric dye which is widely used in textile industries. Its extensive use, poor biodegradability and substantial discharge in water bodies caused an environmental loss and also found lethal to animal and human life. The basic cause for this is its poor biodegradability which might be due to the presence of a number of aromatic rings in these dye molecules where conventional techniques have been unsuccessful for their discoloration and degradation. Hence, investigations of new method are needed which can conduct complete decomposition of dyes [11].

Recent study by Chong *et al.* [12] showed that Photo catalytic degradation of Rhodamine 6G over Ag modified TiO_2 using surface-enhanced Raman scattering technique. The study reveals that silver nanoparticle modified titania nanotubes namely Ag/TiO_2NTs shows excellent photo catalytic degradation of Rh6G in comparison with silver nanoparticles and undoped titania nanoparticles. In another study, photo catalytic degradation of Rhodamine 6G with zinc oxide nanorods synthesized via solution process was reported by Wahab *et al*. where 82% degradation of Rh6G was achieved in 60 minutes [13].Nano-sphere mixed oxides namely $SrCrO_4$ and TiO_2were investigated as catalyst by Ghorai *et al*. for the degradation of Rh6G in aqueous solution under UV light. Study reveals that Strontium Chromium Titanate (SCT) catalyst possesses higher photo catalytic activity than P25 TiO_2 for the oxidation of Rh6G [14].

Sonochemically assisted co-precipitation method for synthesis of ZnO and Nd doped ZnO polyscales for removal of Rhodamine 6G dye under UV light irradiation was reported by Satpal *et al*. [15], where photo catalytic studies showed that the Nd/ZnO samples exhibited excellent photo catalytic activity compared to bare ZnO. However, very less amount of work has been reported on degradation and removal of Rh6G laser dye using Bismuth doped ZnO.

In present study we report the synthesis, characterization of Bismuth doped zinc oxide crystallites (Bi-ZnO) and its photo catalytic performance towards degradation of Rhodamine 6G dye under solar light. The effect of various parameters such as amount of photo catalyst, concentration of dye and pH of medium are also discussed.

2. Experimental

2.1. Materials

Zinc nitrate [$Zn(NO_3)_2$](assay ≥ 98%), Oxalic acid [$(COO)_2.H_2O$](assay 99.5%),Bismuth nitrate pentahydrate [$Bi(NO_3)_3.5H_2O$](assay 99.5%), Rhodamine 6G (assay 99%)and other required chemicals are of analytical grade, obtained from Merck Ltd. Mumbai, India and were used without further purification. The100ppm Rhodamine 6G solution (Rh6G100) was prepared by using double distilled water.

2.2. Preparation of Bi-doped zinc oxide photo catalyst

Bi^{3+}doped ZnO was prepared by parallel flow co precipitation method using Zn $(NO_3)_2$, $(COO)_2.H_2O$ and $Bi(NO_3)_3$ with their aqueous solutions. Zn $(NO_3)_2$, $(COO)_2.H_2O$, desired $Bi(NO_3)_3.5H_2O$ and HNO_3 were completely dissolved in de-ionized water, the molar ratio of Bi/Zn is 0/100, 1/100, 2/100, 3/100, 4/100 and 5/100 respectively. The pH value of precipitation reaction was maintained to around 6.0 by adjusting the flow rate of addition of two solutions. The precipitate formed was filtered and washed with distilled water until no pH change could be detected. It was then dispersed in absolute ethanol and dried in electric oven at 383K for 2 hours. ZnO prepared with different molar ratio of Bi/Zn (0/100, 1/100, 2/100, 3/100, 4/100 and 5/100) were named as ZnO, 1%Bi, 2%Bi, 3%Bi, 4%Bi and 5%Bi respectively. The Bi-doped zinc oxide (BZO) crystallites were obtained by calcination of BZO precursor powders, at 500 °C in air. The undoped zinc oxide (ZO) was also synthesized by calcination of ZO at 500°C for comparison.

2.3. Equipment and light source

Thermal decomposition of ZO and BZO was studied with thermogravimetry (ShimadzuTG-DTG-60H).While, BZO crystallite was characterized by X-ray diffractometer (D-8 Advance Bruker AXS). UV–visible spectra (UV-1601, Shimadzu) and Photoluminescence (PL) spectra (Shimadzu, RF-5301PC) were performed at ambient temperature. The photo catalytic reactions were carried out at ambient temperature under the irradiation of sunlight in batch photo reactor. The details of setup of photo reactor were already explained elsewhere [16]. The initial pH of suspension was recorded with the help of pH meter (EUTECH-pH510).The extent of photo catalytic degradation (PCD)of Rh6G at an interval of 1hr sunlight irradiation was primarily checked by means of decrease in absorbance at 527nm (λmax of Rh6G).Complete mineralization of Rh6G was confirmed by chemical oxygen demand (COD) reduction method. The COD determination tests were performed according to standard dichromate method [17] using COD digester (SPECTRALAB2015M). The PCD efficiency was calculated using the following expression:

$$\eta = (COD_i\text{-}COD_t/COD_i) \times 100 \quad (1)$$

where η is the photo catalytic degradation efficiency,COD_i is the initial chemical oxygen demand and COD_t is the chemical oxygen demand at time t. The intensity of sunlight was checked by ferrioxalate actinometry [18]. The average photon flux calculated for sunlight was found to be1.7×10^{-7} $Einsteins^{-1}$ cm^{-2}.

The reusability of the photo catalyst was evaluated by recalcining the photo catalyst after PCD reaction in the batch mode, washing, drying in electric oven at110°C and using it for Rh6G degradation under identical experimental conditions.

2.4. Photo catalytic degradation experiments

Photo catalytic activity of ZO and BZO in solar light was compared by means of degradation of Rh6G.All the PCD experiments were carried out in replicate and at an ambient temperature, without external supply of oxygen. The detailed procedure of PCD experiments is explained elsewhere [19]. The effect of fluctuation of sunlight intensity was eliminated by simultaneous run of PCD experiments

3. Results and discussion

3.1. TG - DTA study

The main objective of TG–DTA study was to find the minimum possible calcination temperature at which precursor of ZO and Bi doped ZO is converted to respective oxides. The thermal behavior of corresponding precursors of ZO and Bi doped ZO (3%) is presented in Fig. 1.

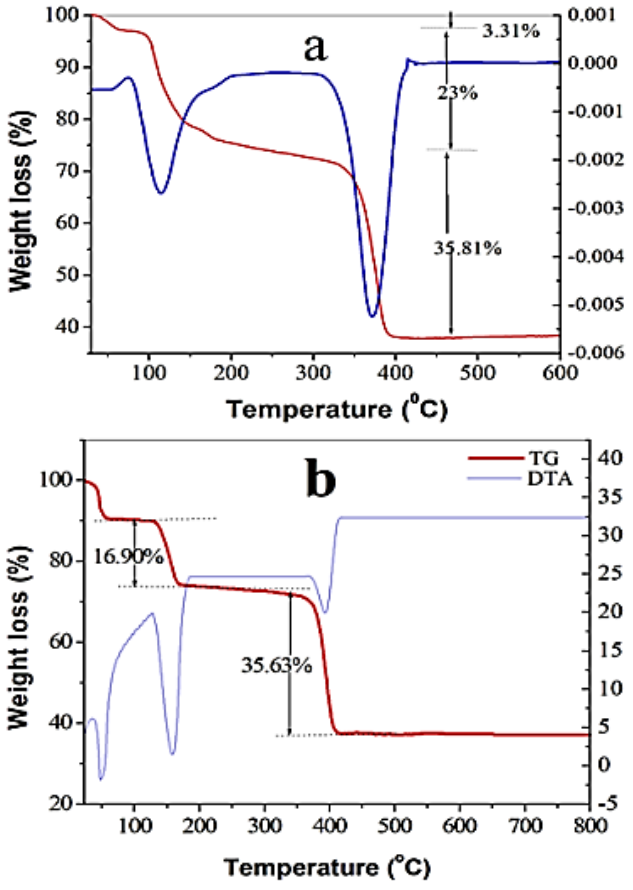

Fig. 1. TG-DTA curves for pure (ZO) and Bi doped zinc oxalate (BZO) precursors (color online)

There are two major weight loss processes from 30°C to 390°C in TG curve of zinc oxalate precursor (Fig. 1a). The weight losses centered at 60°C and 120°C corresponding to a 3.3% and 23% respectively are due to the conversion of zinc oxalate dihydrate to anhydrous zinc oxalate i.e. loss of two water of crystallization molecules. The weight loss of 35.8 % at 340–390°C is attributed to the conversion of anhydrous zinc oxalate to zinc oxide. The DTA curve shows two major peaks corresponding to the weight losses in TGA curve. In case of Bi doped zinc oxalate precursor (Fig.1b), two stage decomposition was noticed, where first weight loss occurred below 100°C(16.90%) and second weight loss observed in the temperature range 390°C to 415°C (35.63%) which was supported by its DTA analysis. There was no weight loss observed above 419°C in both the cases.

From TG-DTA analysis it is confirmed that zinc oxalate and Bi doped zinc oxalate precursors are completely converted in to zinc oxide at 400°C which is further supported by XRD and FT-IR analysis data.

3.2. Characterization of Bi-doped ZnO

3.2.1. XRD pattern

The XRD data was used to investigate the structural properties after incorporation of Bi in the ZnO. Fig. 2 shows XRD pattern of the undoped and Bi doped ZnO.

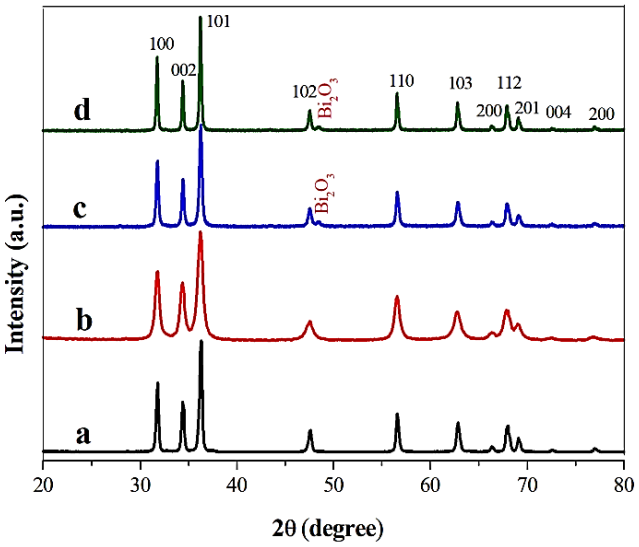

Fig. 2. XRD pattern of pure and Bi-doped zinc oxide (color online)

This analysis reveals the existence of a ZnO single-phase with a hexagonal wurtzite structure. No peak originating from other compounds is detected beside those from ZnO. The XRD patterns show that Bi doping changes the growth orientation of the crystallites which is related to the films nucleation process. The (002) preferential orientation in an undoped ZnO is changed to (100) preferential direction in the Bi doped ZnO which was in accordance with report by Minhong *et al*. [20].We assume here that there is only one phase because the quantity of Bi^{3+}dopant is too small compared to the precursors of Zn and the electro negativity difference between Zn and O is greater than that between Bi and O. All the samples show X-ray diffraction peaks that can be indexed to hexagonal

wurtzite structural ZnO and match well with standard hexagonal ZnO (a = 3.249 Å and c = 5.205 Å, JCPDS Card No. 005-0664). A segregate Bi_2O_3 phase (bismite) is appreciable by increasing the amount of dopant species.

3.2.2. Raman spectra

Raman spectra were recorded with an integral microscope Raman system RFS27 spectrometer equipped with 1024 X 256 pixels liquefied nitrogen-cooled germanium detector. The 1064 nm line of the Nd: YAG laser (red laser) was used to excite the sample. To avoid intensive heating of the sample, the laser power at the sample was kept at15 mW. The Raman spectral patterns of bare ZnO (ZO) and Bi-doped ZnO sample in the 200–800 cm^{-1}spectral range are shown in Fig. 3(a) and (b).

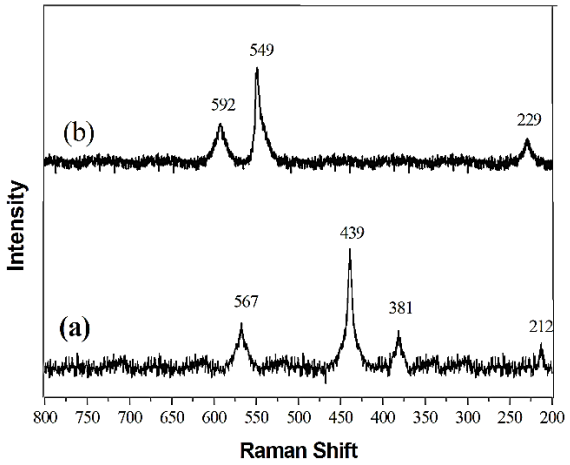

Fig. 3. Raman spectral survey of bare ZnO (a) and Bi-doped ZnO (b)

The spectrum consists of four peaks located at about 212, 381, 439 and 569 cm^{-1}, which correspond to the 2TA; 2E2 (low), A1 (TO), E2 (high) and A1 (LO) fundamental phonon modes of hexagonal ZnO, respectively [21]. Fig. 3b presents the Bi-doped ZnO spectrum which contains of three peaks located at about 229, 549 and 592 cm^{-1} which correspond to the shifted peaks of 2TA, A1(TO) and E1(LO) respectively. A1 (LO) polar branches appeared at about 549 cm^{-1} respectively, on incorporating Bi in ZnO, the A1 (LO) become a sharp peak and shifted about 20 cm^{-1} towards lower energy. The peak at 229 cm^{-1} was attributed to the 2TA; 2E2 (low) mode, which is one of the characteristic peak of Bi-O bonds. The band at 549 cm^{-1} corresponds to A1 symmetry with LO modes. The shifted peaks at 229 attributed to the 2TA; 2E2 (low) and E2 (high) - E2 (low) mode, which is one of the characteristic peak of Bi-O bonds. The shifted peak at 439 cm^{-1} is recognized to the high-E2 mode, which is one of the characteristic peaks of wurtzite ZnO. Above 400 cm^{-1} the peak intensities are increased and few small peaks also observed.

3.2.3. XPS analysis

The composition and chemical states of the elements presents in Bi/ZnO were examined by X-ray photoelectron spectroscopy. The typical X-ray photoelectron spectrum of the Bi/ZnO (3 % BZO) is displayed in Fig. 4.

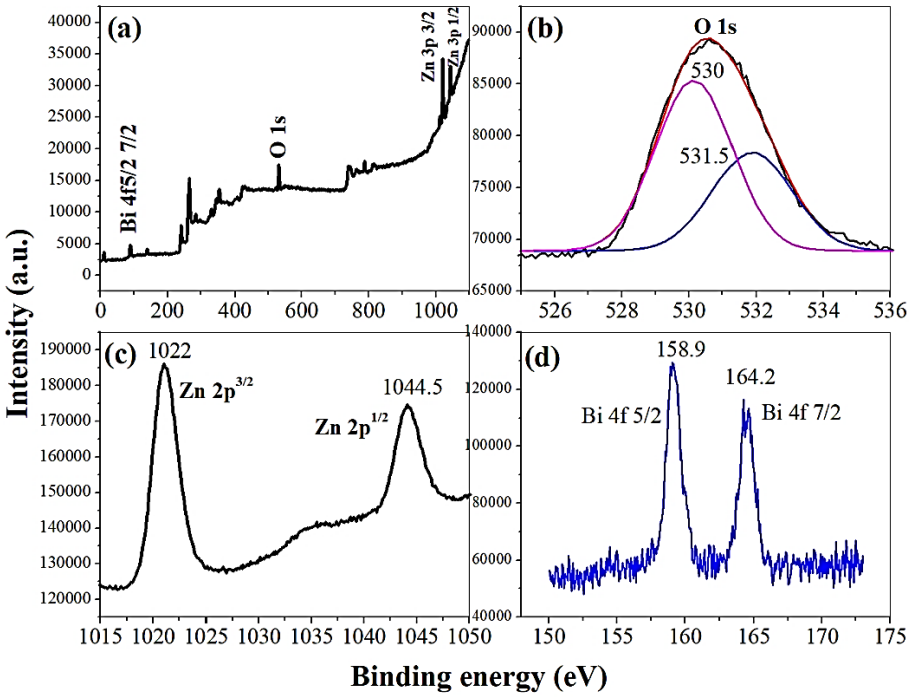

Fig. 4. X-ray photoelectron spectra (XPS) of the Bi-doped ZnO (color online)

This spectrum clearly indicates that, material consists of Zn, Bi and O. The O 1s profile is asymmetric and can be fitted to two symmetrical peaks α and β located at 530 and 531.5 eV, indicating two different kinds of O species in the sample. These peaks should be associated with lattice oxygen of ZnO and chemisorbed oxygen caused by the surface hydroxyl (OH), respectively [22]. XPS spectra of Zn 2p, and the peak positions of Zn 2p 1/2 and Zn 2p 3/2 are located at 1044.5 eV and 1022 eV, we conclude here that Zn is in the state of Zn^{2+}. The peaks of Bi 4f 5/2 and Bi 4f 7/2 are at 158.9 and 164.2 eV reveals that bismuth is in the state of Bi^{3+} [23, 24]

3.2.4 .SEM

The SEM images of bare zinc oxide and Bi-doped ZnO calcined at 500ºC are shown in Fig. 5.

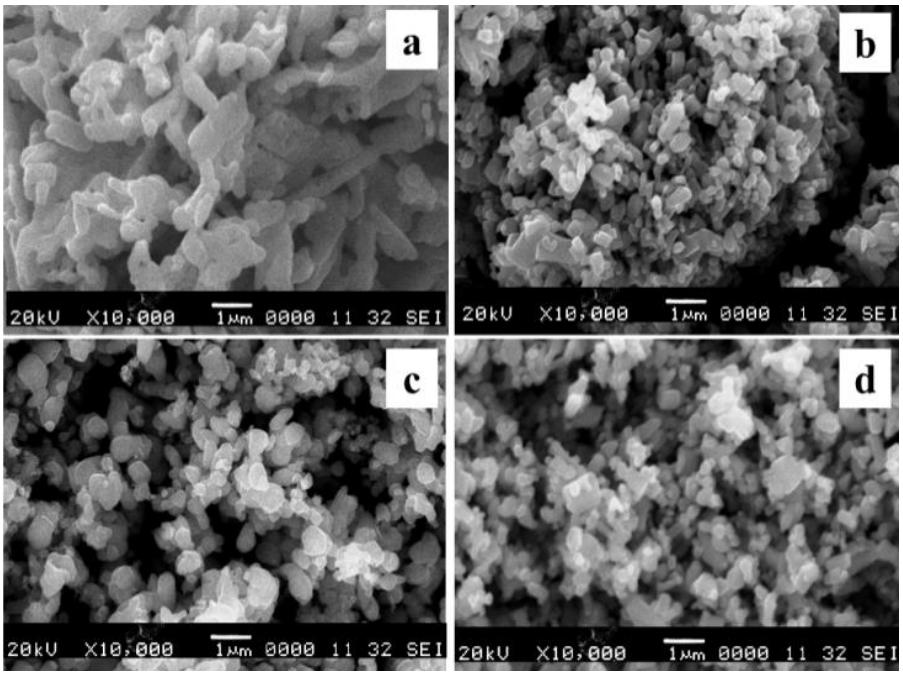

Fig. 5. SEM analysis of undoped and Bi-doped zinc oxide

From this it is clear that Bi^{3+} doping is effective for changing the morphology of ZnO. Among these samples, the SEM image of 3% Bi is having irregular villus-like morphology with abundant pores was observed in the particles, which enhance the surface area.

A representative Energy Dispersive X-ray spectrum (EDX) of Bi-doped ZnO is depicted in Fig. 6.

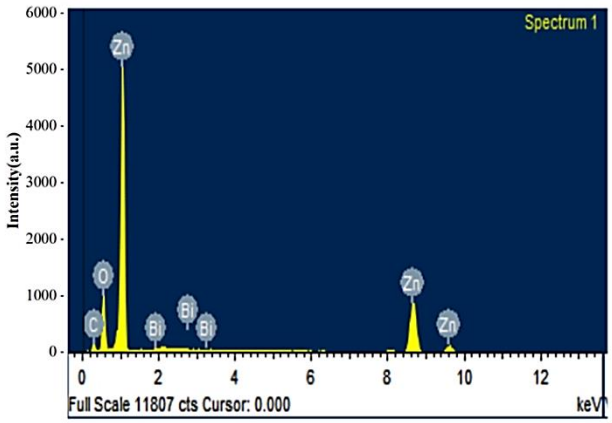

Fig. 6. EDX Spectra of Bi-doped zinc oxide (color online)

It shows peaks corresponding to residual C, Zn, O and Bi. No trace amount of other impurities could be seen in the detection limit of the EDX which also supports the doping of Bismuth in ZnO. This incorporation was found to induce a red shift of the near band gap luminescence. Table 1 demonstrates the elemental composition of the metals detected as per EDX analysis.

Table 1. Elemental Composition of the metals by EDX analysis

Element	**Atomic No.**	**Weight [%]**	**Atom [%]**
Carbon	6	16.70	31.70
Oxygen	8	36.43	51.92
Zinc	30	47.02	16.40
Bismuth	83	-0.15	-0.02
Totals		100.00	100.00

3.2.5. UV-visible spectra

As the samples were prepared for use in photo catalytic reaction, their UV–visible properties may

strongly influence photo catalytic activity. The UV-vis. absorbance spectra of pure and Bi^{3+}doped ZnO is presented in Fig. 7.

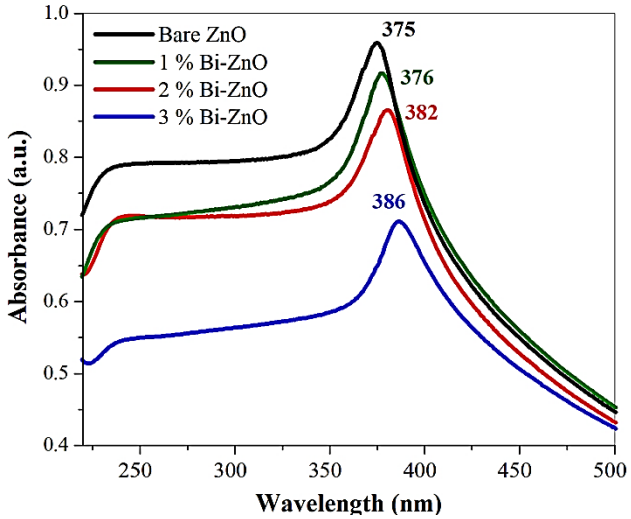

Fig. 7. UV-visible spectra of Bi-doped zinc oxide (color online)

It has been found that there is a red shift in absorption maxima in pure ZnO (375 nm) with increase in mole % of Bi in Bi-ZnO. The gradual increase in absorption maxima as 1% Bi-ZnO (376nm), 2 % Bi-ZnO (382 nm), 3 % Bi-ZnO (386 nm) reveals the decrease in band gap energy of the semiconducting material and hence possible photo catalytic activity in sunlight. Bi^{3+} doped-ZnO appear in the form of new absorption edges, which indicates that some trapping states have been formed with doping by Bi^{3+}cation. This introduces new electronic states into the band of ZnO to form a new lowest unoccupied molecular orbital. Electron trapping by this inter band trap site also can lead to a decrease in electron-hole recombination in the doped catalyst [25], which can promote the photo catalytic activity. However, when concentration of Bi^{3+} is excessively high, the Bi^{3+} would be the center of electron-hole recombination, thereby inhibit the photo catalytic activity.

We have calculated the band gap energies of the synthesized materials by formula 1240 nm/absorption maxima in nm. The obtained band gap energies (Eg) for pure ZnO, 1 % ZnO, 2 % ZnO and 3 % Bi-ZnO were found as 3.30, 3.29, 3.24 and 3.21 eV respectively. The band gap energies (Eg) of the materials were also evaluated by using Tauc equation by plotting $(\alpha h\nu)^2$ in (eV $cm^{-1})^2$ v/s Energy ($h\upsilon$) in eV. Typical linear fittings of the pure ZnO and Bi-doped ZnO are shown in Fig.8. The Eg values were assessed by extrapolating the linear portion of the Tauc plot of $(\alpha h\nu)^2$ v/s photon energy[26,27].The Eg values for the pure ZnO,1 % , 2% and 3% Bi-doped ZnO were 3.32,3.28, 3.25 and 3.21 eV respectively, which are in good agreement with the earlier calculated values. It has been observed that the band gap energy decreased with increasing Bi^{3+} concentrations in ZnO material (Fig.8). This might be originated from the charge transfer between the ZnO valence or conduction band thereby enhancement in the photo catalytic activity of Bi-doped ZnO in the sunlight.

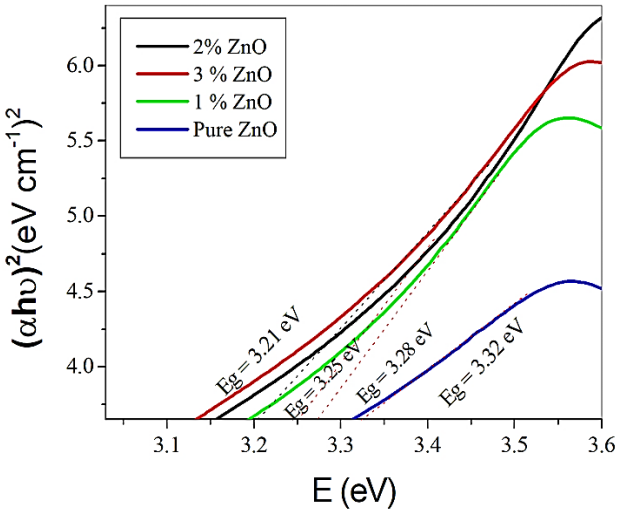

Fig. 8. Band gap energies (Eg) of pure and Bi-doped ZnO materials from TAUC plots (color online)

3.2.6. Photoluminescence study

The photo catalytic activity of a catalyst is usually determined by the efficiency of photo generated electron-hole separation. As photoluminescence originates from the recombination of charge carriers, the PL spectra are highly useful to study the recombination or trapping of charge carriers. Fig. 9 shows the PL spectra for the un-doped zinc oxide and various Bi-doped zinc oxide samples which exhibits the emission in the range 350-550nm.

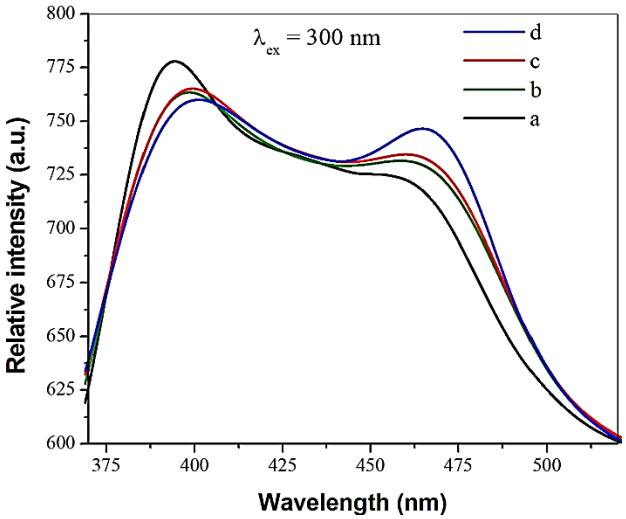

Fig. 9. PL spectra of Bi-doped zinc oxide and bare ZnO (color online)

When compared with un-doped ZnO,it has been observed that, in Bi-doped ZnO sample there is significant reduction in the intensity, which indicates that the Bi-doped zinc oxide sample which lowers the recombination rate of photo generated charge careers. This improves the separation of charge careers thereby increasing the quantum efficiency of the photo catalytic reaction. It is

worth to mention here that, the 1% and 3% Bi-doped zinc oxide samples exhibit a maximum decrease in the PL intensity as compared to 5% Bi-doped zinc oxide sample. As a result, the 1% and 3% samples are promising photo catalyst for degradation of Rh6G.The acceptor energy level of bismuth dopant is found to be 0.13 eV above valance band. The binding energy between the acceptor and the excitation measured as a function of temperature was found to be 14 MeV. A hole concentration of 5.36 × $10^{18}cm^{-3}$ and a mobility of 8.9 $cm^2/(V.s)$ was reported for 3% bismuth-doped ZnO[28].

This study suggests that bismuth is an excellent dopant to obtain stable and reproducible p-type conductivity in ZnO which finds application in optoelectronic devices. The origin of the first band is related with band-edge emission (recombination of free excitations between conduction band and valence band), reported [29]. Second, much broader emission band extending from 450 to 484 nm results most probably from the presence of defects. The recently prevailing opinion is that the green luminescence in ZnO is originating from the photo generated hole recombination with electron at the singly ionized oxygen vacancy [30].

3.2.7. FTIR of Bi-doped zinc oxide and bare ZnO

A representative FTIR spectra of the pure ZnO and various Bi doped ZnO samples is shown in Fig. 10.

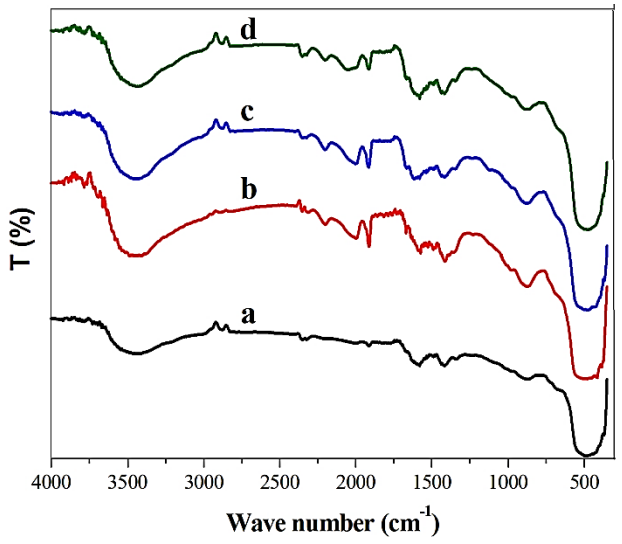

Fig. 10. FTIR spectra of Bi-doped zinc oxide and bare ZnO (color online)

In the FTIR spectrum for pristine ZnO (Fig. 10a), the peak at 3366 cm^{-1} corresponds to the OH group. The sharp peak at 1629 cm^{-1} is assigned to C=O stretching that might be due to the presence of precursor. The peak at 471cm^{-1} arises due to the Bi-O stretching present in ZnO. The characteristic peaks for the 1 % BZO sample observed at 3446 cm^{-1},1637 and 471 cm^{-1}were attributed to the presence of OH,C=O and Bi-O in the photo catalyst respectively (Fig. 10b). There was similar trend noticed for 3% and 5% BZO samples (Fig. 10c, d). The doped Bi is significantly presented by Bi-O stretching frequency peak emerged in Bi-ZnO samples around 866 cm^{-1} and is not seen in bare ZnO. The residual OH in the material appeared as a broad peak around 3448 cm^{-1} which is a essential condition to enhance photo catalytic activity by easier generation of hydroxyl radicals in sunlight.

3.3. Solar photo catalytic activity of Bi-doped zinc oxide

We have chosen Rhodamine 6G (Rh6G) as model dye and solar light to evaluate the photocatlytic activity of the Bi-doped ZnO photo catalyst. The optimum amount of catalyst dose and the molar concentration of the Bi dopant required for the photo catalytic reaction were also studied. The photo catalytic activity of the Bi^{3+}-doped ZnO photo catalysts in comparison with bare zinc oxide is shown in Fig. 11.

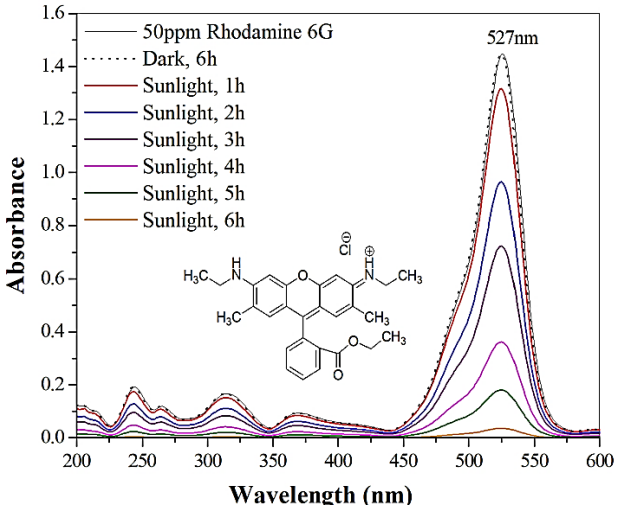

Fig. 11. Solar photocatalytic degradation of Rhodamine 6G over Bi-doped ZnO (color online)

The optimum catalyst dose was determined by conducting the photcatalytic degradation of Rh6G in the aqueous medium with varied doses of Bi-doped ZnO catalysts from 25mg to 200mg per $100cm^3$ of 50 ppm dye solution under similar experimental conditions. In absence of photo catalyst no detectable degradation of dye was noticed. Bi^{3+}-doped ZnO photo catalysts exhibit better photo catalytic activity than ZnO and the 3% Bi-ZnO possesses the best photo catalytic activity among the experimented compositions. These results suggest that Bi^{3+} doping (Bi <5 %) enhances the photo catalytic activity of ZnO and that there is an optimum loading of Bi^{3+} ions in ZnO crystallites. As expected, the maximum degradation rate was noticed with 3% BZO catalyst where Rh6G was 80% degraded within 6hr., because of the maximum emission of the spectral response into the visible region and the suppression of electron and hole recombination. The red shift in 1%, 2%, 4% and 5% samples were compared to the 3% BZO sample which explains the reason why they show lesser degradation efficiency as

compared to 3% BZO photo catalyst. As Rh6G exhibits an absorption band around 527nm, undoped ZnO degrades almost 45 % of Rh6G because of dye sensitization. The catalytic activities were found to increase as the molar ratio of Bi: Zn was increased from 0 to 3%. This enhancement in the photo catalytic activity upon doping ZnO with Bi^{3+} may be attributed to the high specific surface area, inhibition of the electron and hole recombination by Bi species doped in ZnO and increase in absorption of visible light as in PL spectra and UV-vis. spectra respectively.

3.4. The mechanism of photo catalytic degradation of Rh6G over Bi-doped ZnO

When the Bi-doped ZnO photo catalyst was exposed to solar light, a photon energy of higher or equal to the band gap ($h\upsilon \geq E_{bg}$) , causes excitation of electrons into the conduction band (CB) of ZnO generating a positively charged hole in the valence band(h^+) and negative charge in the conduction band as per Eq. 2

$$BiZnO \xrightarrow{h\upsilon} Bi^{3+}(h^+) + ZnO(e^-) \quad (2)$$

$$HO^- + h^+ \longrightarrow HO\cdot \quad (3)$$

$$O_2 + e^- \longrightarrow O_2^{\cdot -} \quad (4)$$

$$O_2^{\cdot -} + H^+ \longrightarrow HO_2\cdot$$
$$HO_2\cdot + e^- \longrightarrow HO_2^-$$
$$HO_2^- + H^+ \longrightarrow H_2O_2$$
$$H_2O_2 + e^- \longrightarrow HO^- + HO\cdot \quad (5)$$

$$Rh_6G + HO\cdot \longrightarrow CO_2 + H_2O + \text{simple molecules} \quad (6)$$

The chemisorbed H_2O molecules interact with holes in the valence band forming $HO\cdot$ radicals (Eq.3), simultaneously an equal number of holes are generated in the 6s level of Bi^{3+} which are taken by the adsorbed O_2 present on the surface of ZnO generating $O_2^{\cdot -}$ (Eq.4).The subsequent reactions of HO^- and $O_2^{\cdot -}$can also generate powerful oxidizing species(Eq.5), hydroxyl radicals($HO\cdot$) which degrade the harmful Laser dye(Rh6G) completely into simple molecules(Eq.6).High charge separation rate is beneficial to form hydroxyl radical, which in turn favors the degradation phenomenon. The earlier studies have proposed that the Bi^{3+} (6s) level is highly important in reducing the energy band gap of TiO_2, which lies between the Bi^{3+} 6s band and the Ti^{4+} 3d band [31]. This leads to the absorption of lower energy photons, leading to an enhancement in the photo catalytic quantum efficiency.

Thus the photo catalytic cycle comprise three main steps

i) Exposure of photo catalyst to induce a transition of electrons from the valence band (VB) to the conduction band (CB), leaving an equal number of vacant sites (holes).

ii) The excited electrons and holes on Bi ion migrate to ZnO surface, thereby facilitating the charge separation and higher photo catalytic efficiency. This charge separation phenomenon is revealed by the reduction of PL intensity of the proposed catalytic material when compared with ZnO. This process accumulates electrons and holes in Bi and ZnO respectively. To prevent the recombination of electron-hole pairs, Bismuth on the ZnO surface acts as a barrier and causes effective electron-hole pair separation at the heterojunction interfaces significantly which improve the photo catalytic performance of the photo catalyst.

iii) The $HO\cdot$ radical which is usually accepted as the main reactive species responsible for the degradation of organic dye. Where the photo generated electrons might react with oxygen molecule adsorbed on the surface of Bi-ZnO to yield $O_2\cdot$

3.5. Reuse of photo catalyst

The reuse of Bi-doped ZnO was separately studied, by keeping all other parameters constant. During this study, after sunlight irradiation for 6hrs, photo reaction mixture was centrifuged and filtered. Filtrate was used for COD determination and residue was washed several times with double distilled water followed by filtration and drying at 110°C in an electric oven. Recovered Bi-doped ZnO was then reused for new PCD batch, without any further treatment such as heating in any kind of furnace etc. Activity of recycled Bi-doped ZnO was found to retain even after fourth photo degradation experiment.

4. Conclusions

In present study (Bi doped ZnO) BZO and ZO (Zinc oxide) was synthesized by simple precipitation method. The incorporation of Bi^{3+}in ZnO was supported by broadening and lower Bragg angle shift in XRD pattern of the samples as compare to that of pure ZnO. The band gap energy (Eg) of pure ZnO (3.32 eV) becomes narrower for BZO (3.21eV) as observed in UV-visible spectra and estimated from Tauc plots. This is also supported by XPS analysis demonstrating Zn is in the state of $Zn^{2+}$and Bi is in the state of Bi^{3+}.The room temperature PL spectrum supports the number of defects and hence oxygen vacancies in BZO, which are correlated with its photo catalytic performance towards degradation of Rh6G.

References

[1] Y. W. Chen, Q. Qiao, Y. C. Liu, G. L. Yang, J. Phys. Chem. C **113**, 7497 (2009).
[2] L. Li, W. Wang, H. Liu, X. Liu, Q. Song, S. Ren, J. Phys. Chem.C **113**, 8460 (2009).
[3] N. Kislov, J. Lahiri, H. Verma, D. Y. Goswami, E. Stefanakos, M. Batzill, Langmuir **25**, 3310 (2009).
[4] S. Baruah, S. K. Pal, J. Dutta, Nanosci. Nanotechnol. Asia **2**, 90 (2012).
[5] Z. Meng, Z. Juan, Global Environ. Policy Japan **12**, 1 (2008).

[6] J. Zhao, L. Wang, X. Yan, Y. Yang, Y. Lei, J. Zhou, Y. Huang, Y. Gu, Y. Zhang, Mate. Res. Bull. **46**, 1207 (2011).
[7] H. Abdul, M. Tiziano, G. Valentina, P. Fornasiero, J. Am. Chem. Soc. **130** 9658 (2008).
[8] Y. Hu, Y. Cao, P. Wang, D. Li, W. Chen, Y. He, X. Fu, Y. Shao, Y. Zheng, Appl. Catal. B **125**, 294 (2012).
[9] S. Bagwasi, Y. Niu, M. Nasir, B. Tian, J. Zhang, Appl. Surf. Sci. **264**, 139 (2013).
[10] P. Qu, J. Zhao, T. Shen, H. Hidaka, J. Mol. Catal A **12**, 257 (1998).
[11] I. K. Konstantinou, T. A. Albanis, Appl. Catal. B Environ. **49**, 1 (2004).
[12] X. Chonga, B. Zhao, R. Li, W. Ruan, X. Yang, Colloids and Surfaces A: Physicochem. Eng. Aspects **481**, 7 (2015).
[13] R. Wahab, F. Khan, Journal of Electronic Materials **43**, 4266 (2014).
[14] T. K. Ghorai, N. Biswas, J. Mater. Res. Technol. **2**, 10 (2013).
[15] S. B. Satpal, A. A. Athawale, Mater. Res. Express **5**(8), 085501 (2018).
[16] S. K. Pardeshi, A. B. Patil, Sol. Energy. **82**, 700 (2008).
[17] J. T. Bellaire, G. A. Parr-Smith, Standard methods for the examination of water and Waste water, Seventh ed., American Public Health Association, Washington DC, 1985.
[18] C. G. Hatchard, C. A. Parker, Proc. R. Soc. London, A **235**, 518 (1956).
[19] A. B. Patil, K. R. Patil, S. K. Pardeshi, J. Hazard, Materials **183**, 315 (2010).
[20] M. Jiang, X. Liu, J. Mater. Sci.: Mater. Electron. **20**, 972 (2009).
[21] R. S. Zeferino, M. B. Flores, U. Pall, J. Appl. Phys. **109**, 014308 (2011).
[22] J. F. Moudler, W. F. Stickle, P. E. Sobol, K. D. Bomben, Handbook of X-ray Photoelectron Spectroscopy, Perkin-Elmer, Eden Prairie, MN, 191 (1992).
[23] Y. Schuhl, H. Baussart, R. Delobel, M. Le Bras, J. Leroy, L. G. Gengembre J. Rimblot, J. Chem. Soc., Faraday Trans. **79**, 2055 (1983).
[24] X. Jing-Jing, C. Min-Dong, F. De-Gang, Trans. Nonferrous Met. Soc. China. **21**, 340 (2011).
[25] K. R. Jakkidi, S. Basavaraju, D. K. Valluri, Chem. Catal. Chem. **14**, 492 (2009).
[26] H. A. Oualid, O. Amadine, Y. Essamlali, K. Daanoun, M. Zahouily, RSC Adv. **8**, 20737 (2018).
[27] R. M. Jagtap, D. R. Kshirsagar, V. H. Khire, S. K. Pardeshi, Journal of Solid State Chemistry **276**, 194 (2019).
[28] J. W. Lee, N. G. Subramaniam, J. C. Lee, S. Kumar, T. W. Kang, A Letters Journal Exploring the Frontiers of Physics **95**, 47002 (2011).
[29] A. B. Djuri, Y. H. Leung, Small. **2**, 944 (2006).
[30] W. F. Yao, H. Wang, X. H. Xu, X. F. Cheng, J. Huang, S. X. Shang, X. N. Yang, M. Wang, Appl. Catal. A **243**, 185 (2003).
[31] H. Mizoguchi, K. Ueda, H. Kawazoe, H. Hosono, T. Omata, S. Fujitsu, J. Mater. Chem.**7**, 943 (1997).

* Corresponding author: satish.pardeshi@unipune.ac.in
skpardeshi@gmail.com